Generation of undamped exciton-biexciton beats in InAs quantum dots using six-wave mixing

H. Tahara, Y. Ogawa, and F. Minami
Department of Physics, Tokyo Institute of Technology, Oh-Okayama 2-12-1, Tokyo 152-8551, Japan

K. Akahane and M. Sasaki
National Institute of Information and Communications Technology, 4-2-1 Nukui-kitamachi, Koganei, Tokyo 184-8795, Japan
(Received 11 August 2013; revised manuscript received 12 March 2014; published 21 May 2014)

We report the generation of undamped exciton-biexciton beats for coherent dynamics of excitons in InAs quantum dots at telecommunication wavelengths. The exciton-biexciton beat is damped rapidly in four-wave mixing measurements, but a six-wave mixing technique with three excitation pulses enables us to regenerate and control the exciton-biexciton beat perfectly. We have demonstrated the complete regeneration of the exciton-biexciton beat by adjusting the delay time between the first and second excitation pulses. This approach is different from conventional coherent control in quantum dots. Furthermore, the initial phase of the exciton-biexciton beat is controlled by using this technique. We show that the generation of undamped beats is a powerful tool for controlling quantum states.

DOI: 10.1103/PhysRevB.89.195306 PACS number(s): 78.67.Hc, 42.50.Md, 78.47.nj

Coherent control of quantum states is actively being investigated for the study of quantum information processing. Electron spin states and Rabi oscillations of excitons have been controlled in optical and transport measurements [1–4]. Four-wave mixing (FWM) has been used for coherent control of excitons in semiconductors [5–8]. Originally, the FWM technique was used for the measurement and control of coherent processes including beat structures in the time domain. Excitonic beat structures were observed as quantum beats of heavy-hole and light-hole excitons [9,10], scattering processes between excitons and phonons [6,8,11], and exciton-biexciton beats [7,12]. Microscopic quantum dynamics clearly shows the periodic shifts of quantum states. However, it is difficult to use the beat structures for quantum information processing because control over a long period of time is forbidden by the damping of the beat amplitudes. Such amplitudes are enhanced or suppressed by using a coherent control technique based on phase-locked pulses [5–8], but the damping is fundamentally unavoidable. Perfect suppression of such damping has not yet been achieved. The damping degrades the controllability for the quantum states, and hence the suppression of the damping is a prerequisite for quantum state control over a sufficient time period.

It is also important to preserve the quantum states of electrons in storage media for quantum information processing. Recently, the photon echo signals in FWM measurements have been applied to solid-state storage [13]. The storage of a time-bin qubit and an optical pulse at the single-photon level has been demonstrated in rare-earth-doped solids [14,15]. The photon echo technique is of interest as a method for storing and retrieving input optical pulses. The essential feature of the photon echo measurement is the rephasing of the polarizations in media with inhomogeneous broadening of the resonance energy, i.e., time reversal. Input pulses are stored until the rephasing time, which is set by the arrival time of the read pulse. Taking full advantage of the photon echo feature, it is possible to generate coherently controlled quantum states that can be stored for a long time without the loss of controllability. Excitons in semiconductor quantum dots (QDs) show fairly long coherence times compared to those in bulk [16]. Studies of excitons in QDs have focused on their usage as long-lived coherent states in solids, but the loss of controllability has not yet been solved. The perfect control of quantum states in QDs, especially biexciton states, is an important step for the realization of quantum memories in solid state media, because biexcitons generate entangled photon pairs [17,18].

In this paper, we show the undamped exciton-biexciton beat generated by six-wave mixing (SWM) in self-assembled InAs QDs. The technique presented in this study differs from conventional three-pulse photon echo measurements, which are widely being used to accurately analyze third-order nonlinear processes [19–21]. We used three-pulse excitation to control the damping of the beat in fifth-order nonlinear processes. The exciton-biexciton beat in semiconductor QDs disappears for long delay times in the FWM measurements [12,22,23], but the beat is regenerated completely in the SWM measurements. This study is a demonstration of the undamped exciton-biexciton beat in QDs.

The investigated sample was grown on a InP(311)B substrate by molecular beam epitaxy. The sample contains 60 layers of InAs self-assembled QDs separated by 20-nm-thick $In_{1-x-y}Ga_xAl_yAs$ spacers. Highly stacked InAs QDs are realized by the strain-compensation technique [24,25]. The exciton states in the QDs were split into X and Y excitons due to the fine-structure splitting. The X and Y excitons were excited in the linear polarization along the $[01\bar{1}]$ and $[\bar{2}33]$ directions, respectively [23]. In this study, the excitation pulses were performed with Y-polarized linear polarization in order not to excite X excitons. The sample was mounted in a closed-cycle refrigerator at 3.4 K. For FWM and SWM measurements, optical pulses were generated by an optical parametric oscillator pumped by a mode-locked Ti:sapphire laser tuned to the exciton resonance wavelength of 1470 nm. The pulse duration was 130 fs, and the repetition rate was 76 MHz. The first, second, and third excitation pulses were incident on the sample with wave vectors $\boldsymbol{k}_1$, $\boldsymbol{k}_2$, and $\boldsymbol{k}_3$, respectively. For the FWM measurements, the third excitation pulse was not used; the FWM (SWM) signal in the direction

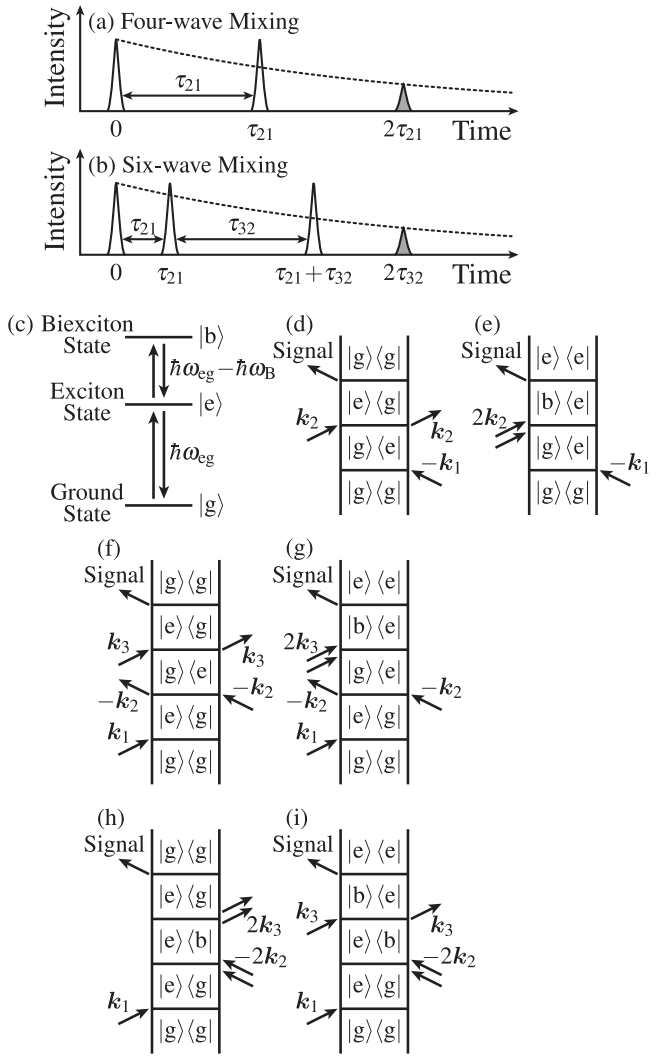

FIG. 1. Illustration of the time development of the excitation processes in (a) four-wave mixing and (b) six-wave mixing measurements. The first, second, and third excitation pulses are incident at 0, τ_{21}, and $\tau_{21}+\tau_{32}$, respectively. Photon echo signals appear at $2\tau_{21}$ and $2\tau_{32}$ in four-wave mixing and six-wave mixing measurements, respectively. The signal intensities obey the exponential decay of excitonic polarization (dotted lines). (c) Energy structure of ground ($|g\rangle$), exciton ($|e\rangle$), and biexciton ($|b\rangle$) states. Transition processes are shown by double-sided Feynman diagrams for (d),(e) four-wave mixing and (f)–(i) six-wave mixing.

of $2\boldsymbol{k}_2-\boldsymbol{k}_1$ ($2\boldsymbol{k}_3-2\boldsymbol{k}_2+\boldsymbol{k}_1$) was detected by a photodetector in transmission geometry.

The time development of excitation processes in FWM and SWM measurements is shown in Figs. 1(a) and 1(b). The excitonic polarizations generated by the first excitation pulse disappear rapidly due to the phase difference caused by the inhomogeneous broadening of the exciton resonance energy. The second excitation pulse begins the reversal of the phase evolution at τ_{21}. This reversal of the phase shifts takes the same duration as the delay between the two excitation pulses; the rephased photon echo signal appears at a time of $2\tau_{21}$ in FWM measurements. In contrast, the photon echo signal in SWM measurements does not appear before the third excitation. After the first rephasing at $2\tau_{21}$, the third excitation pulse begins to reverse the phase evolution again; the reversal occurs until the second rephasing. Eventually, the rephased photon echo signal appears at $2\tau_{32}$ in SWM measurements. The dephasing of the FWM signal is proportional to $e^{-(4/T_2)\tau_{21}}$, where T_2 is the dephasing time of excitons. In contrast, the SWM signal is proportional to $e^{-(4/T_2)\tau_{32}}$, because the rephasing time $2\tau_{21}$ in FWM measurements is replaced by the rephasing time $2\tau_{32}$ in SWM measurements. The excitonic transitions in QDs are explained by the three-level system shown in Fig. 1(c). The resonance energy of biexciton transition, $\hbar\omega_{eg}-\hbar\omega_B$, is smaller than that of exciton transition, $\hbar\omega_{eg}$, by the biexciton binding energy $\hbar\omega_B$. The FWM processes are illustrated by double-sided Feynman diagrams in Figs. 1(d) and 1(e). The interference between exciton and biexciton transitions causes the beat with a period of $T_B=2\pi/\omega_B$. In the SWM measurements, the SWM signals are composed of four transition processes illustrated in Figs. 1(f)–1(i).

The experimental result of the FWM measurement is shown in Fig. 2(a). The excitons in QDs show long coherence times because the coherent states of excitons are protected by the confinement potential of the QDs [16,22]. The dephasing time T_2 is obtained to be 0.8 ns. In the time range of 0 to 6 ps, the exciton-biexciton beat was observed as shown in Fig. 2(b). The beat period T_B is obtained to be 1.16 ps, which corresponds to the biexciton binding energy. Here, it

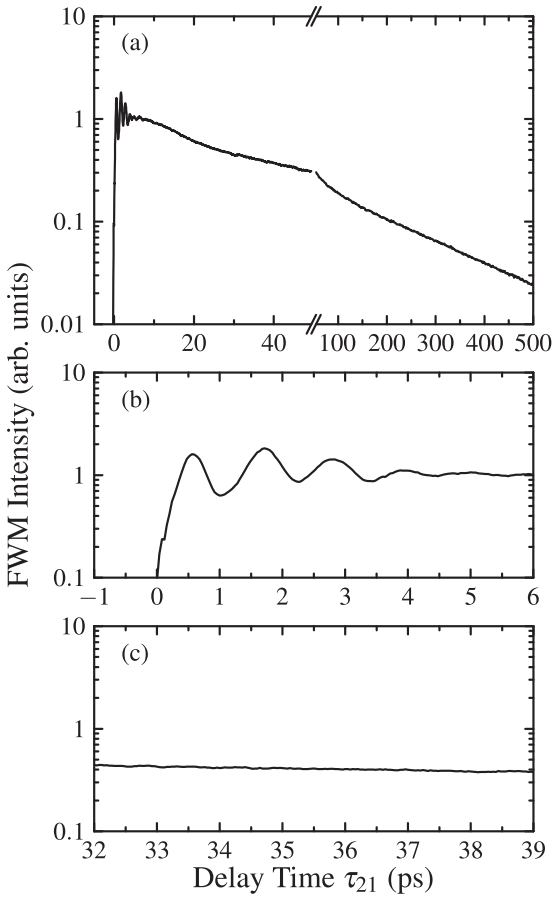

FIG. 2. Four-wave mixing intensity at delay times of (a) 0 to 500 ps, (b) 0 to 6 ps, and (c) 32 to 39 ps.

should be noted that the period is modulated slightly by the fine-structure splitting energy [22,23]. Each QD has a different biexciton binding energy because the energy is determined by the confinement potential of the corresponding QD. Therefore, the beat exhibits the damping due to the inhomogeneous broadening of the biexciton binding energy. Calculating the diagrams in Figs. 1(d) and 1(e), the FWM intensity in the direction of $2\boldsymbol{k}_2 - \boldsymbol{k}_1$ is expressed as

$$I_{\mathrm{FWM}}(\tau_{21}) \propto \Theta(\tau_{21}) e^{-(4/T_2)\tau_{21}} \left| 2 - C_{\mathrm{B}} e^{i\omega_{\mathrm{B}}\tau_{21}} e^{-(\sigma_{\mathrm{B}}^2/4)\tau_{21}^2} \right|^2, \quad (1)$$

where ω_{B} is the frequency of the exciton-biexciton beat, σ_{B} is the linewidth of the inhomogeneous broadening of the biexciton binding energy, C_{B} is the beat amplitude, and $\Theta(t)$ is a step function. The detailed derivation of Eq. (1) is explained in the Appendixes. The signal from the exciton (biexciton) transition is expressed by the first (second) term as illustrated in Fig. 1(d) [Fig. 1(e)]. It is assumed that the difference between the dephasing times of the exciton and biexciton is sufficiently negligible because the time development depending on the difference varies slowly compared to the damping factor $e^{-(\sigma_{\mathrm{B}}^2/4)\tau_{21}^2}$ [23]. The biexcitonic polarization is opposite in sign to the excitonic polarization because of the difference between the final states. The phase shift due to the biexciton binding energy is not reversed in the FWM process; the interference of the exciton and biexciton states is observed at the rephasing time $2\tau_{21}$ as the exciton-biexciton beat. In the FWM measurement, the exciton-biexciton beat cannot be observed after a delay time of 10 ps, owing to the effect of the damping factor $e^{-(\sigma_{\mathrm{B}}^2/4)\tau_{21}^2}$, as shown in Fig. 2(c). The manipulability of the quantum state is limited to the time range before damping. The technique for suppression of the damping is necessary to control the quantum states in the exciton-biexciton beat for long delay times. Then, SWM measurements with three excitation pulses were performed to eliminate the damping of the beat.

In the SWM measurements, the diffracted signal in the direction of $2\boldsymbol{k}_3 - 2\boldsymbol{k}_2 + \boldsymbol{k}_1$ is determined by two delay times τ_{21} and τ_{32}, as shown in Fig. 1(b). Compared to the rephasing time $2\tau_{21}$ in the FWM measurements, the SWM signal appears at the rephasing time $2\tau_{32}$. It should be noted that the rephasing time is independent of the delay time τ_{21}. The delay time τ_{21} is adjusted to control the exciton-biexciton beat as explained in the following. In order to explain the role of the delay time τ_{21}, the experimental results of the SWM measurements for $\tau_{21} =$ 0.0 ps are shown in Figs. 3(a) and 3(b) by the black lines. The exciton-biexciton beat in the SWM measurements is similar to that in the FWM measurements, as shown in Figs. 2(b) and 2(c). The exciton-biexciton beat was observed within the delay time of 10 ps. The damping of the exciton-biexciton beat is caused by the inhomogeneous broadening of the biexciton binding energy, as it is for the FWM signal. For long delay times τ_{21} and τ_{32}, the exciton-biexciton beat is caused by the interference between the transition processes illustrated in Figs. 1(f) and 1(g). The processes illustrated in Figs. 1(h) and 1(i) disappear due to the damping. Using the same expansion approach to nonlinear response as conventionally used for FWM signals [26,27], the SWM intensity is obtained from the fifth-order terms in the density matrix. The detailed derivation of theoretical SWM intensity is explained in the Appendixes.

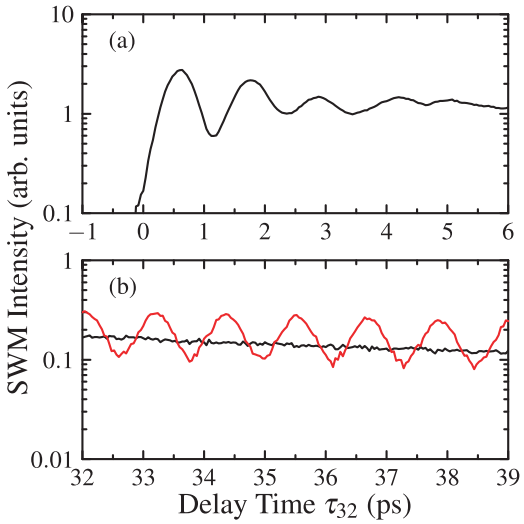

FIG. 3. (Color online) Six-wave mixing intensity at delay times of (a) 0 to 6 ps and (b) 32 to 39 ps. The black lines show the results for $\tau_{21} = 0.0$ ps. The red line shows the result for τ_{21} obeying Eq. (3).

Calculating the diagrams in Figs. 1(f) and 1(g), the SWM intensity in the direction of $2\boldsymbol{k}_3 - 2\boldsymbol{k}_2 + \boldsymbol{k}_1$ is expressed as

$$I_{\mathrm{SWM}}(\tau_{32},\tau_{21}) \propto \Theta(\tau_{32}-\tau_{21})\Theta(\tau_{32})\Theta(\tau_{21}) e^{-(4/T_2)\tau_{32}} \times \left| 2 - C_{\mathrm{B}} e^{i\omega_{\mathrm{B}}(\tau_{32}-\tau_{21})} e^{-(\sigma_{\mathrm{B}}^2/4)(\tau_{32}-\tau_{21})^2} \right|^2. \quad (2)$$

This result is well explained by comparing to the FWM intensity in Eq. (1). The dephasing is expressed by $e^{-(4/T_2)\tau_{32}}$, because the rephasing time $2\tau_{21}$ in FWM measurements is replaced by $2\tau_{32}$ in SWM measurements. The interference of excitonic and biexcitonic signals occurs due to the phase evolution in time from biexciton excitation to signal emission. In the FWM processes, the exciton-biexciton beating factor is determined by τ_{21}, which is the time interval from the second excitation at τ_{21} to the rephasing at $2\tau_{21}$. In contrast, the beat in the SWM processes depends on $\tau_{32} - \tau_{21}$. This is the time interval from the third excitation at $\tau_{21} + \tau_{32}$ to the rephasing at $2\tau_{32}$.

The damping of the exciton-biexciton beat is eliminated by adjusting the delay time τ_{21} in a way that depends on the delay time τ_{32}. The exciton-biexciton beat is regenerated even for long delay times because an appropriate shift of the delay time τ_{21} eliminates the damping. In the regeneration technique, the delay time τ_{21} is chosen according to the following condition:

$$\tau_{21} = nT_{\mathrm{B}} \ \text{ for } \left(\frac{1}{2}+n\right)T_{\mathrm{B}} \leqslant \tau_{32} < \left(\frac{3}{2}+n\right)T_{\mathrm{B}}, \quad (3)$$

where n is an integer. Substituting this condition into Eq. (2), the SWM intensity is expressed as

$$I_{\mathrm{SWM}}(\tau_{32}) \propto \Theta(\tau_{32}) e^{-(4/T_2)\tau_{32}} \left| 2 - C_{\mathrm{B}} e^{i\omega_{\mathrm{B}}\tau_{32}} \right|^2. \quad (4)$$

This equation represents the undamped exciton-biexciton beat. Even if the delay time τ_{32} is set to be long, the exciton-biexciton beat can be observed by adjusting the long delay time τ_{21}. The damping of the exciton-biexciton beat due to the long delay time τ_{32} is canceled by increasing the delay time τ_{21}. We performed this condition for the SWM measurements by adjusting the delay times such as $\tau_{21} = 31.32$ ps ($n = 27$)

for 31.90 ps $\leqslant \tau_{32} <$ 33.06 ps and $\tau_{21} = 32.48$ ps ($n = 28$) for 33.06 ps $\leqslant \tau_{32} <$ 34.22 ps. The experimental result of the SWM intensity under the condition of Eq. (3) is shown in Fig. 3(b) by the red line. The exciton-biexciton beat cannot be observed for the time range of 32 to 39 ps in the FWM measurements, but the beat is regenerated for long delay times in the SWM measurements. The invariant amplitude of the beat shows the complete elimination of the damping. This regeneration technique is effective up to longer delay times scaled by T_2.

This regeneration technique was also used to control the initial phase of the exciton-biexciton beat, θ_i, by modifying the selection procedure for τ_{21} from Eq. (3) to the following condition:

$$\tau_{21} = nT_B + \frac{\theta_i}{\omega_B}$$
$$\text{for } \left(\frac{1}{2}+n\right)T_B + \frac{\theta_i}{\omega_B} \leqslant \tau_{32} < \left(\frac{3}{2}+n\right)T_B + \frac{\theta_i}{\omega_B}. \quad (5)$$

The initial phase of the beat is determined by the offset θ_i/ω_B in this shifted form of the delay time τ_{21}. In this condition, the SWM intensity is expressed as

$$I_{SWM}(\tau_{32}) \propto \Theta(\tau_{32}) e^{-(4/T_2)\tau_{32}} \left|2 - C_B e^{-i\theta_i} e^{i\omega_B \tau_{32}}\right|^2. \quad (6)$$

The initial phase is expressed by the factor $e^{-i\theta_i}$, where the exciton-biexciton beat becomes out of phase at $\tau_{32} = 0$ for the condition $\theta_i = 0$. The initial phase is manipulated by changing the condition of the delay time τ_{21}. Control of the initial phase was performed by adjusting the delay times such as $\tau_{21} = 31.32$, 31.61, 31.90, and 32.19 ps for $\theta_i = 0$, $\pi/2$, π, and $3\pi/2$, respectively, to measure the intensity at the delay time $\tau_{32} = 33$ ps. The experimental results, shown in Fig. 4, demonstrate clear $\pi/2$ shifts of the initial phase of the exciton-biexciton beat. The initial phase was successfully controlled by an appropriate offset of the delay time τ_{21}. It should be noted that the rephasing time of the photon echo signal is determined by the delay time τ_{32}, which is independent of the delay time τ_{21} controlling the initial phase. Even if the measurement uses a fixed delay time τ_{32}, the interference of the exciton and biexciton states is controlled by this shift of the delay time τ_{21}. The advantage of the SWM measurements with such shifts is not only the complete elimination of the damping but also the multiple degrees of control allowed by two independent delay times.

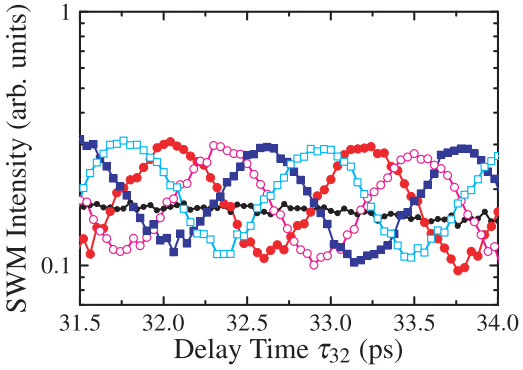

FIG. 4. (Color online) Six-wave mixing intensity for the initial phases of $\theta_i = 0$ (solid circle), $\pi/2$ (open circle), π (solid square), and $3\pi/2$ (open square). The result for $\tau_{21} = 0.0$ ps is shown as a black line.

In conclusion, we have demonstrated the regeneration and control of the exciton-biexciton beat in the quantum dot ensemble using a six-wave mixing technique. The damping of the exciton-biexciton beat cannot be suppressed in four-wave mixing, but appropriate timing of the excitation pulses in six-wave mixing enables us to eliminate the damping. We have clearly shown that the conditional six-wave mixing measurement is a powerful technique for the control of quantum states. The presented technique is compatible with a decoherence control technique for fundamental dephasing processes [28,29]. By combining these techniques, the controllability of quantum state becomes almost unlimited. This study for quantum dot ensemble is an important demonstration to realize perfect quantum memories in solid. It is also applicable to a wide range of other quantum beats, e.g., complicated beats in multilevel systems. We believe that this technique for eliminating the problem of damping will allow the measurement of many heretofore hidden fundamental beating phenomena.

This work was supported by the Global Center of Excellence Program by MEXT, Japan through the Nanoscience and Quantum Physics Project of the Tokyo Institute of Technology. H.T. was supported by a Grant-in-Aid for JSPS Fellows.

APPENDIX A: THEORETICAL FOUR-WAVE MIXING SIGNAL FOR THE EXCITON-BIEXCITON SYSTEM

The theoretical nonlinear response is obtained by solving the equation of motion for the density matrix [26,27]. We use a three-level density matrix to represent the exciton-biexciton system. The density matrix is written as ρ_{ij} $(i,j = \text{g,e,b})$, where the ground, exciton, and biexciton states are denoted by g, e, and b, respectively. The equation of motion for the density matrix is expressed as

$$\frac{\partial \rho}{\partial t} = -\frac{i}{\hbar}[H,\rho] \quad (A1)$$

with

$$H = H_0 + H_1, \quad (A2)$$

$$H_0 = \begin{pmatrix} \hbar\omega_{gg} & 0 & 0 \\ 0 & \hbar\omega_{ee} & 0 \\ 0 & 0 & \hbar\omega_{bb} \end{pmatrix}, \quad (A3)$$

$$H_1 = \begin{pmatrix} 0 & -\mu_{ge}E^* & 0 \\ -\mu_{eg}E & 0 & -\mu_{eb}E^* \\ 0 & -\mu_{be}E & 0 \end{pmatrix}, \quad (A4)$$

where the unperturbed Hamiltonian H_0 shows the eigenenergies in the absence of excitation fields; the eigenenergies of the ground, exciton, and biexciton states are denoted by $\hbar\omega_{gg}$, $\hbar\omega_{ee}$, and $\hbar\omega_{bb}$, respectively. The energy differences $\hbar\omega_{ee} - \hbar\omega_{gg}$ and $\hbar\omega_{bb} - \hbar\omega_{ee}$ are denoted by $\hbar\omega_{eg}$ and $\hbar\omega_{eg} - \hbar\omega_B$, respectively, where $\hbar\omega_B$ is the biexciton binding energy. The light-matter interaction Hamiltonian H_1 represents the exciton

and biexciton transitions. The dipole moment between the ground and exciton (exciton and biexciton) states is denoted by $\mu_{\rm ge}$ ($\mu_{\rm eb}$), where the complex conjugate is expressed as $\mu_{\rm eg}=\mu_{\rm ge}^{*}$ ($\mu_{\rm be}=\mu_{\rm eb}^{*}$). The electric field for two-pulse excitation is expressed as $E=\sum_{j=1,2}E_j(t)e^{i\boldsymbol{k}_j\cdot\boldsymbol{r}-i\omega_{\rm eg}(t-t_j)}$, where $\boldsymbol{k}_j$ and t_j are the wave vector and the arrival time of the jth excitation pulse, respectively. The frequency of incident light is adjusted to match the exciton resonance. The excitation pulses are assumed to be delta-function pulses, i.e., $E_j(t)\propto\delta(t-t_j)$.

In order to express the coherent dynamics of the exciton-biexciton system, the decay terms should be taken into account. The equation of motion for the nth-order density matrix $\rho^{(n)}$, which is proportional to the nth power of the electric field, is expressed as

$$\frac{\partial\rho_{\rm gg}^{(n)}}{\partial t}=-\frac{i}{\hbar}\left(H_{\rm ge}\rho_{\rm eg}^{(n-1)}-\rho_{\rm ge}^{(n-1)}H_{\rm eg}\right)+\frac{1}{T_1}\rho_{\rm ee}^{(n)}, \quad \text{(A5)}$$

$$\frac{\partial\rho_{\rm ee}^{(n)}}{\partial t}=-\frac{i}{\hbar}\left(H_{\rm eg}\rho_{\rm ge}^{(n-1)}-\rho_{\rm eg}^{(n-1)}H_{\rm ge}+H_{\rm eb}\rho_{\rm be}^{(n-1)}-\rho_{\rm eb}^{(n-1)}H_{\rm be}\right)-\frac{1}{T_1}\rho_{\rm ee}^{(n)}+\frac{1}{T_1'}\rho_{\rm bb}^{(n)}, \quad \text{(A6)}$$

$$\frac{\partial\rho_{\rm bb}^{(n)}}{\partial t}=-\frac{i}{\hbar}\left(H_{\rm be}\rho_{\rm eb}^{(n-1)}-\rho_{\rm be}^{(n-1)}H_{\rm eb}\right)-\frac{1}{T_1'}\rho_{\rm bb}^{(n)}, \quad \text{(A7)}$$

$$\frac{\partial\rho_{\rm eg}^{(n)}}{\partial t}=-\frac{i}{\hbar}\left(H_{\rm eg}\rho_{\rm gg}^{(n-1)}-\rho_{\rm ee}^{(n-1)}H_{\rm eg}+H_{\rm eb}\rho_{\rm bg}^{(n-1)}\right)-i\omega_{\rm eg}\rho_{\rm eg}^{(n)}-\frac{1}{T_2}\rho_{\rm eg}^{(n)}, \quad \text{(A8)}$$

$$\frac{\partial\rho_{\rm be}^{(n)}}{\partial t}=-\frac{i}{\hbar}\left(H_{\rm be}\rho_{\rm ee}^{(n-1)}-\rho_{\rm bg}^{(n-1)}H_{\rm ge}-\rho_{\rm bb}^{(n-1)}H_{\rm be}\right)-i(\omega_{\rm eg}-\omega_{\rm B})\rho_{\rm be}^{(n)}-\frac{1}{T_2'}\rho_{\rm be}^{(n)}, \quad \text{(A9)}$$

$$\frac{\partial\rho_{\rm bg}^{(n)}}{\partial t}=-\frac{i}{\hbar}\left(H_{\rm be}\rho_{\rm eg}^{(n-1)}-\rho_{\rm be}^{(n-1)}H_{\rm eg}\right)-i(2\omega_{\rm eg}-\omega_{\rm B})\rho_{\rm bg}^{(n)}-\frac{1}{T_2''}\rho_{\rm bg}^{(n)}, \quad \text{(A10)}$$

where H_{ij} is a matrix element of the total Hamiltonian H. The decay times of $\rho_{\rm ee}$, $\rho_{\rm bb}$, $\rho_{\rm eg}$, $\rho_{\rm be}$, and $\rho_{\rm bg}$ are phenomenologically introduced as T_1, T_1', T_2, T_2', and T_2'', respectively. The nth-order density matrix $\rho^{(n)}$ is calculated from the $(n-1)$th-order density matrix $\rho^{(n-1)}$, where the initial state corresponds to the ground state $\rho_{\rm gg}^{(0)}\neq 0$, i.e., $\rho_{\rm ee}^{(0)}=\rho_{\rm bb}^{(0)}=\rho_{\rm eg}^{(0)}=\rho_{\rm be}^{(0)}=\rho_{\rm bg}^{(0)}=0$.

The four-wave mixing (FWM) signal is calculated from the off-diagonal elements of the third-order density matrix, i.e., $\mu_{\rm ge}\rho_{\rm eg}^{(3)}+\mu_{\rm eb}\rho_{\rm be}^{(3)}$. The first (second) term corresponds to the FWM signal illustrated in Fig. 1(d) [Fig. 1(e)]. In the investigated quantum dot (QD) ensemble, each QD has a different resonance energy because each resonance energy is determined by the confinement potential of the corresponding QD. To calculate the theoretical FWM signal, the inhomogeneous broadening of the resonance energy should be taken into account. The inhomogeneous broadening of the exciton resonance energy is assumed to be a Gaussian distribution given by $g(\omega)=(A_{\rm eg}/\sqrt{\pi}\sigma_{\rm eg})e^{-(\omega-\bar{\omega}_{\rm eg})^2/\sigma_{\rm eg}^2}$ with a magnitude $A_{\rm eg}$, a central value $\hbar\bar{\omega}_{\rm eg}$, and a linewidth $\hbar\sigma_{\rm eg}$ [26]. Using this distribution, the FWM signal with the inhomogeneous broadening is given by $P_{\rm FWM}(t)=\int d\omega_{\rm eg}g(\omega_{\rm eg})(\mu_{\rm ge}\rho_{\rm eg}^{(3)}+\mu_{\rm eb}\rho_{\rm be}^{(3)})$. The inhomogeneous broadening of the biexciton binding energy causes the damping in the exciton-biexciton beat. This inhomogeneous broadening, as well as that of the exciton resonance energy, is assumed to be a Gaussian distribution: $g_{\rm B}(\omega)=(A_{\rm B}/\sqrt{\pi}\sigma_{\rm B})e^{-(\omega-\bar{\omega}_{\rm B})^2/\sigma_{\rm B}^2}$. Taking into account this distribution, the exciton-biexciton beat factor $e^{i\omega_{\rm B}t}$ is replaced by $e^{i\bar{\omega}_{\rm B}t}e^{-(\sigma_{\rm B}^2/4)t^2}$. The damping factor $e^{-(\sigma_{\rm B}^2/4)t^2}$ is determined by the linewidth of the inhomogeneous broadening. The FWM signal in the direction of $2\boldsymbol{k}_2-\boldsymbol{k}_1$ is expressed as

$$P_{\rm FWM}(t)\propto\Theta(t-t_2)\Theta(t_2-t_1)e^{i(2\boldsymbol{k}_2-\boldsymbol{k}_1)\cdot\boldsymbol{r}}e^{-i\bar{\omega}_{\rm eg}(t-2t_2+t_1)}\times e^{-(\sigma_{\rm eg}^2/4)(t-2t_2+t_1)^2}e^{-(1/T_2)(t-t_1)}\times\left(2-C_{\rm B}e^{i\bar{\omega}_{\rm B}(t-t_2)}e^{-(\sigma_{\rm B}^2/4)(t-t_2)^2}\right), \quad \text{(A11)}$$

where $\Theta(t)$ is a step function; the beat amplitude $C_{\rm B}$ corresponds to $A_{\rm B}|\mu_{\rm eb}|^2/|\mu_{\rm ge}|^2$. The difference between the dephasing times of the exciton and biexciton is assumed to be sufficiently negligible because the damping factor $e^{-(\sigma_{\rm B}^2/4)(t-t_2)^2}$ decreases much faster than the time development depending on the difference between the dephasing times. The rephasing time, i.e., photon echo generation, is expressed by the factor $e^{-(\sigma_{\rm eg}^2/4)(t-2t_2+t_1)^2}$, which is caused by the inhomogeneous broadening of the exciton resonance energy. Since the inhomogeneous broadening in the QD ensemble is considerably larger than the spectral linewidth of the excitation pulses, the linewidth $\hbar\sigma_{\rm eg}$ is determined by the linewidth of the excitation pulses [23]. Therefore, the photon echo signal exhibits a delta-function shape at $t=2t_2-t_1$ due to the factor $e^{-(\sigma_{\rm eg}^2/4)(t-2t_2+t_1)^2}$. In FWM measurements, the time-integrated signal is measured as a function of the delay time $\tau_{21}=t_2-t_1$. The FWM intensity $I_{\rm FWM}(\tau_{21})=\int dt|P_{\rm FWM}(t)|^2$ is expressed as

$$I_{\rm FWM}(\tau_{21})\propto\Theta(\tau_{21})e^{-(4/T_2)\tau_{21}}\left|2-C_{\rm B}e^{i\bar{\omega}_{\rm B}\tau_{21}}e^{-(\sigma_{\rm B}^2/4)\tau_{21}^2}\right|^2. \quad \text{(A12)}$$

Since the rephasing time is $2\tau_{21}$, the dephasing factor is measured as the exponential decay $e^{-(4/T_2)\tau_{21}}$. The exciton-biexciton beat factor $e^{i\bar{\omega}_{\rm B}\tau_{21}}e^{-(\sigma_{\rm B}^2/4)\tau_{21}^2}$ is also determined by the delay time τ_{21}.

APPENDIX B: THEORETICAL SIX-WAVE MIXING SIGNAL FOR THE EXCITON-BIEXCITON SYSTEM

The six-wave mixing (SWM) signal is also calculated from the equation of motion for the density matrix. In the calculation, the electric field for three-pulse excitation is expressed as $E=\sum_{j=1,2,3}E_j(t)e^{i\boldsymbol{k}_j\cdot\boldsymbol{r}-i\omega_{\rm eg}(t-t_j)}$. The SWM signal is obtained from the off-diagonal elements of the fifth-order density matrix, i.e., $P_{\rm SWM}(t)=\int d\omega_{\rm eg}g(\omega_{\rm eg})(\mu_{\rm ge}\rho_{\rm eg}^{(5)}+\mu_{\rm eb}\rho_{\rm be}^{(5)})$, where the inhomogeneous broadening of the exciton resonance energy is taken into account. The first (second) term

is composed of the SWM signals illustrated in Figs. 1(f) and 1(h) [Figs. 1(g) and 1(i)]. The SWM signal in the direction of $2\boldsymbol{k}_3 - 2\boldsymbol{k}_2 + \boldsymbol{k}_1$ is expressed as

$$\begin{aligned} P_{\mathrm{SWM}}(t) \propto{}& \Theta(t-t_3)\Theta(t_3-t_2)\Theta(t_2-t_1) \\ &\times e^{i(2\boldsymbol{k}_3-2\boldsymbol{k}_2+\boldsymbol{k}_1)\cdot\boldsymbol{r}} e^{-i\bar{\omega}_{\mathrm{eg}}(t-2t_3+2t_2-t_1)} \\ &\times e^{-(\sigma_{\mathrm{eg}}^2/4)(t-2t_3+2t_2-t_1)^2} e^{-(1/T_2)(t-t_1)} \\ &\times \big(4 - 2C_{\mathrm{B}} e^{i\bar{\omega}_{\mathrm{B}}(t-t_3)} e^{-(\sigma_{\mathrm{B}}^2/4)(t-t_3)^2} \\ &+ C_{\mathrm{B}} e^{-i\bar{\omega}_{\mathrm{B}}(t_3-t_2)} e^{-(\sigma_{\mathrm{B}}^2/4)(t_3-t_2)^2} \\ &- 2C'_{\mathrm{B}} e^{i\bar{\omega}_{\mathrm{B}}(t-2t_3+t_2)} e^{-(\sigma_{\mathrm{B}}^2/4)(t-2t_3+t_2)^2}\big), \end{aligned} \tag{B1}$$

where the beat amplitude C'_{B} corresponds to $A_{\mathrm{B}}|\mu_{\mathrm{eb}}|^4/|\mu_{\mathrm{ge}}|^4$. The inhomogeneous broadening of the biexciton binding energy is taken into account in the exciton-biexciton beat. The first, second, third, and fourth terms correspond respectively to the SWM signals illustrated in Figs. 1(f), 1(g), 1(h), and 1(i). The photon echo signal exhibits a delta-function shape at $t = 2t_3 - 2t_2 + t_1$ due to the factor $e^{-(\sigma_{\mathrm{eg}}^2/4)(t-2t_3+2t_2-t_1)^2}$. In SWM measurements, the time-integrated signal $I_{\mathrm{SWM}}(\tau_{32},\tau_{21}) = \int dt |P_{\mathrm{SWM}}(t)|^2$ is measured as a function of the first and second delay times, which are denoted by $\tau_{21} = t_2 - t_1$ and $\tau_{32} = t_3 - t_2$, respectively. The SWM intensity is expressed as

$$\begin{aligned} I_{\mathrm{SWM}}(\tau_{32},\tau_{21}) \propto{}& \Theta(\tau_{32}-\tau_{21})\Theta(\tau_{32})\Theta(\tau_{21}) e^{-(4/T_2)\tau_{32}} \\ &\times \big|4 - 2C_{\mathrm{B}} e^{i\bar{\omega}_{\mathrm{B}}(\tau_{32}-\tau_{21})} e^{-(\sigma_{\mathrm{B}}^2/4)(\tau_{32}-\tau_{21})^2} \\ &+ C_{\mathrm{B}} e^{-i\bar{\omega}_{\mathrm{B}}\tau_{32}} e^{-(\sigma_{\mathrm{B}}^2/4)\tau_{32}^2} \\ &- 2C'_{\mathrm{B}} e^{-i\bar{\omega}_{\mathrm{B}}\tau_{21}} e^{-(\sigma_{\mathrm{B}}^2/4)\tau_{21}^2}\big|^2. \end{aligned} \tag{B2}$$

For long delay times compared to the damping of the exciton-biexciton beat, i.e., $2/\sigma_{\mathrm{B}} \ll \tau_{21}, \tau_{32}$, the SWM intensity is expressed as

$$\begin{aligned} I_{\mathrm{SWM}}(\tau_{32},\tau_{21}) \propto{}& \Theta(\tau_{32}-\tau_{21})\Theta(\tau_{32})\Theta(\tau_{21}) e^{-(4/T_2)\tau_{32}} \\ &\times \big|2 - C_{\mathrm{B}} e^{i\bar{\omega}_{\mathrm{B}}(\tau_{32}-\tau_{21})} e^{-(\sigma_{\mathrm{B}}^2/4)(\tau_{32}-\tau_{21})^2}\big|^2. \end{aligned} \tag{B3}$$

Since the rephased photon echo appears at $2\tau_{32}$, the dephasing of the SWM signal is determined by the second delay time τ_{32}. It is expressed by the exponential decay $e^{-(4/T_2)\tau_{32}}$. In contrast, the exciton-biexciton beat depends on the difference between the first and second delay times, i.e., $\tau_{32} - \tau_{21}$.

[1] B. Patton, U. Woggon, and W. Langbein, Phys. Rev. Lett. **95**, 266401 (2005).

[2] A. Greilich, R. Oulton, E. A. Zhukov, I. A. Yugova, D. R. Yakovlev, M. Bayer, A. Shabaev, Al. L. Efros, I. A. Merkulov, V. Stavarache, D. Reuter, and A. Wieck, Phys. Rev. Lett. **96**, 227401 (2006).

[3] R. Hanson, L. P. Kouwenhoven, J. R. Petta, S. Tarucha, and L. M. K. Vandersypen, Rev. Mod. Phys. **79**, 1217 (2007).

[4] H. Kosaka, T. Inagaki, Y. Rikitake, H. Imamura, Y. Mitsumori, and K. Edamatsu, Nature (London) **457**, 702 (2009).

[5] A. P. Heberle, J. J. Baumberg, and K. Köhler, Phys. Rev. Lett. **75**, 2598 (1995).

[6] M. U. Wehner, M. H. Ulm, D. S. Chemla, and M. Wegener, Phys. Rev. Lett. **80**, 1992 (1998).

[7] T. Voss, I. Rückmann, J. Gutowski, V. M. Axt, and T. Kuhn, Phys. Rev. B **73**, 115311 (2006).

[8] Y. Ogawa and F. Minami, Phys. Rev. B **75**, 073302 (2007).

[9] K. Leo, T. C. Damen, J. Shah, E. O. Göbel, and K. Köhler, Appl. Phys. Lett. **57**, 19 (1990).

[10] S. Schmitt-Rink, D. Bennhardt, V. Heuckeroth, P. Thomas, P. Haring, G. Maidorn, H. Bakker, K. Leo, D.-S. Kim, J. Shah, and K. Köhler, Phys. Rev. B **46**, 10460 (1992).

[11] L. Bányai, D. B. Tran Thoai, E. Reitsamer, H. Haug, D. Steinbach, M. U. Wehner, M. Wegener, T. Marschner, and W. Stolz, Phys. Rev. Lett. **75**, 2188 (1995).

[12] T. F. Albrecht, K. Bott, T. Meier, A. Schulze, M. Koch, S. T. Cundiff, J. Feldmann, W. Stolz, P. Thomas, S. W. Koch, and E. O. Göbel, Phys. Rev. B **54**, 4436 (1996).

[13] A. L. Alexander, J. J. Longdell, M. J. Sellars, and N. B. Manson, Phys. Rev. Lett. **96**, 043602 (2006).

[14] M. U. Staudt, S. R. Hastings-Simon, M. Nilsson, M. Afzelius, V. Scarani, R. Ricken, H. Suche, W. Sohler, W. Tittel, and N. Gisin, Phys. Rev. Lett. **98**, 113601 (2007).

[15] B. Lauritzen, J. Minář, H. de Riedmatten, M. Afzelius, N. Sangouard, C. Simon, and N. Gisin, Phys. Rev. Lett. **104**, 080502 (2010).

[16] P. Borri, W. Langbein, S. Schneider, U. Woggon, R. L. Sellin, D. Ouyang, and D. Bimberg, Phys. Rev. Lett. **87**, 157401 (2001).

[17] R. M. Stevenson, R. J. Young, P. Atkinson, K. Cooper, D. A. Ritchie, and A. J. Shields, Nature (London) **439**, 179 (2006).

[18] N. Akopian, N. H. Lindner, E. Poem, Y. Berlatzky, J. Avron, D. Gershoni, B. D. Gerardot, and P. M. Petroff, Phys. Rev. Lett. **96**, 130501 (2006).

[19] T. Joo, Y. Jia, J.-Y. Yu, M. J. Lang, and G. R. Fleming, J. Chem. Phys. **104**, 6089 (1996).

[20] H. Lee, Y.-C. Cheng, and G. R. Fleming, Science **316**, 1462 (2007).

[21] S. G. Carter, Z. Chen, and S. T. Cundiff, Phys. Rev. B **76**, 121303(R) (2007).

[22] W. Langbein, P. Borri, U. Woggon, V. Stavarache, D. Reuter, and A. D. Wieck, Phys. Rev. B **70**, 033301 (2004).

[23] H. Tahara, Y. Ogawa, F. Minami, K. Akahane, and M. Sasaki, Phys. Rev. B **87**, 035304 (2013).

[24] K. Akahane, N. Ohtani, Y. Okada, and M. Kawabe, J. Cryst. Growth **245**, 31 (2002).

[25] K. Akahane, N. Yamamoto, and T. Kawanishi, Phys. Status Solidi A **208**, 425 (2011).

[26] T. Yajima and Y. Taira, J. Phys. Soc. Jpn. **47**, 1620 (1979).

[27] H. Haug and S. W. Koch, *Quantum Theory of the Optical and Electronic Properties of Semiconductors*, 5th ed. (World Scientific, Singapore, 2009).

[28] M. Sasaki, A. Hasegawa, J. Ishi-Hayase, Y. Mitsumori, and F. Minami, Phys. Rev. B **71**, 165314 (2005).

[29] T. Kishimoto, A. Hasegawa, Y. Mitsumori, J. Ishi-Hayase, M. Sasaki, and F. Minami, Phys. Rev. B **74**, 073202 (2006).